Journal of Non-Crystalline Solids 404 (2014) 26–31

Contents lists available at ScienceDirect

Journal of Non-Crystalline Solids

journal homepage: www.elsevier.com/ locate/ jnoncrysol

Crystallization behavior of sodium iron phosphate glass $Na_{2-x}Fe_{1+0.5x}P_2O_7$ for sodium ion batteries

Tsuyoshi Honma *, Atsushi Sato, Noriko Ito, Takuya Togashi, Kenji Shinozaki, Takayuki Komatsu

Department of Materials Science and Technology, Nagaoka University of Technology, Kamitomioka 1603-1, Nagaoka, Niigata 940-2188, Japan

ARTICLE INFO

Article history:
Received 5 June 2014
Received in revised form 10 July 2014
Available online xxxx

Keywords:
Sodium ion batteries;
Glass-ceramics;
Sodium iron phosphate;
$Na_2FeP_2O_7$

ABSTRACT

Crystallization behavior of precursor glass in the system of sodium iron phosphate $Na_{2-x}Fe_{1+0.5x}P_2O_7$ was examined. We obtained homogeneous precursor glasses in the composition range between $x = 0$ and 0.77. The formation of triclinic $P\bar{1}$ phase, which plays active material for sodium ion batteries, was confirmed in whole composition. Precipitation of $Na_4P_2O_7$ was confirmed except for the $P\bar{1}$ phase by means of XRD analysis in $x = 0$ that means $Na_2FeP_2O_7$ is thermally unstable, meanwhile a pure $P\bar{1}$ phase was obtained in $x = 0.44$, which corresponds to stoichiometric $Na_{3.12}Fe_{2.44}(P_2O_7)_2$. We propose that the optimal composition exists around $x = 0.44$ not $x = 0$ ($Na_2FeP_2O_7$) to form the $P\bar{1}$ phase with high volume fractions.

1. Introduction

Recently sodium ion batteries are considered to be an alternative to lithium ion batteries, which require precious resources such as lithium, cobalt, nickel, and copper, due to natural abundance of sodium. The concept of sodium ion batteries is not so novel. Actually Na_xCoO_2 [1,2], active materials are reported so far. Furthermore, $NaFeO_2$ [3], $Na_{2/3}(Ni_{1/3}Mn_{2/3})O_2$ [4], $Na(Ni_{1/3}Fe_{1/3}Mn_{1/3})O_2$ [5], $Na_{2/3}(Fe_{1/2}Mn_{1/2})O_2$, [6] and $NaNiO_2$ [7] and so many kinds of layer type cathodes are also proposed. In particular, $Na_{2/3}(Fe_{1/2}Mn_{1/2})O_2$ [6] exhibits 190 mAh/g discharge capacity that is almost identical to that of typical material in lithium ion batteries. However, layered rock salt oxides have some problems in mass production. The primary reason of difficulty is their chemical activities for moisture. Even in laboratory use α-$NaFeO_2$ and its related materials must be quenched in a dry Ar filled globe box after calcination process to avoid decomposition by hydration.

On the other hand, recently, poly-anion type $Na_3V_2(PO_4)_3$ [8], Na_2FePO_4F [9], $Na_3V_2(PO_4)_2F_3$ [10] and $Na_4Fe_3(PO_4)_2(P_2O_7)$ [11] are also reported as cathode active materials in sodium half cells. These materials are promising stable and safety batteries as the same as $LiFePO_4$ in Li ion batteries. In 2012, we found triclinic $P\bar{1}$ type $Na_2FeP_2O_7$, which plays cathode as 3.0 V and 91 mAh/g in sodium cells [12–14]. Later some groups also reported on the electrochemical performance of $Na_2FeP_2O_7$, which is obtained from solid state reaction [15–19]. $Na_2FeP_2O_7$ exhibits good cyclic performance [17,18] as well as chemical stability in aqueous solution electrolyte [19]. We are also proposing the glass-ceramic processing (i.e., crystallization of glasses), which is a nice technique, to prepare sodium iron phosphates $Na_2FeP_2O_7$ as well as $LiFePO_4$ [20–22], $LiFe_xMn_{1-x}PO_4$ [23], $Li_3V_2(PO_4)_3$ [24] and $LiVOPO_4$ [25] reported in the previous studies. We also applied the glass-ceramic technique to fabricate $SnO–P_2O_5$ glass anodes for both lithium and sodium ion batteries [26,27]. The advantages in the glass-ceramics route for the fabrication of phosphate-based cathode active materials are: (1) inexpensive raw materials such as α-Fe_2O_3 are used as starting materials [20], (2) both crystallization and carbon coating process can be achieved simultaneously through one step [21] and (3) ferromagnetic impurity phase such as Fe_2P is not formed. Comparing with conventional solid state reaction, it is expected that the compositional distribution is extremely homogeneous in precursor glass, consequently, providing a good cyclic performance [22]. In this paper, we focus on the structure of $P\bar{1}$ type $Na_2FeP_2O_7$. Angenault et al. [28] found sodium partial substitution between Na(3) and Fe(3) site and proposed the precise chemical composition as $Na_{3.12}Fe_{2.44}(P_2O_7)_2$ (ICDD #01-083-0225), which deviates from the starting composition with Na:Fe:P = 2:1:2. If the substitution of Na(3) site by Fe(3) site is available continuously, the general formula and electrochemical reaction will be able to express as Eq (1).

$$Na_{2-x}Fe(II)_{1+0.5x}P_2O_7 \leftrightarrow Na_{1-1.5x}Fe(III)_{1+0.5x}P_2O_7 + (1+0.5x)\left\{Na^+ + e^-\right\}. \quad (1)$$

The theoretical discharge capacity can be calculated as 97 mAh/g in $Na_2FeP_2O_7$ ($x = 0$) and 118 mAh/g in $Na_{3.12}Fe_{2.44}(P_2O_7)_2$ ($x = 0.44$), if the electrochemical reaction progresses between the discharge (Fe^{2+}) and charge (Fe^{3+}) states of Fe ions. The aim of this study is, therefore, to investigate the crystallization behavior of sodium iron phosphate glasses with the chemical compositions of $Na_{2-x}Fe_{1+0.5x}P_2O_7$ and to

* Corresponding author.
E-mail address: honma@mst.nagaokaut.ac.jp (T. Honma).

http://dx.doi.org/10.1016/j.jnoncrysol.2014.07.028
0022-3093/

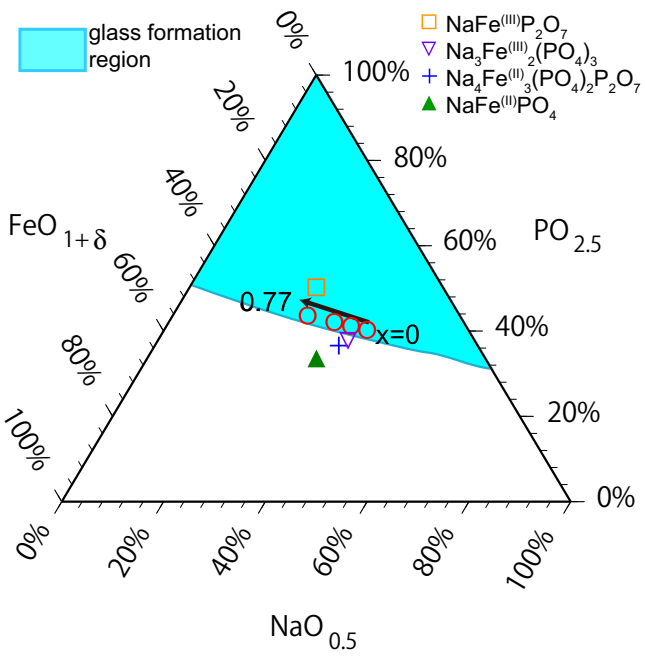

Fig. 1. Glass compositions (open red circle) examined in the sodium iron phosphate system. The glass forming region and typical cathode candidates reported so far are also shown. (For interpretation of the references to color in this figure legend, the reader is referred to the web version of this article.)

clarify electrochemical properties of their glass-ceramic cathode as sodium ion batteries.

2. Experimental procedure

As introduced in Eq. (1), we determined the series of precursor glasses as $Na_{2-x}Fe_{1+0.5x}P_2O_7$ ($x = 0$, 0.22, 0.44, and 0.77). Precursor glasses were fabricated by a conventional melt-quenching method. Starting reagents $NaPO_3$ (97%, Nakarai tesque Co.), α-Fe_2O_3 (99.9%, Kojyundo chemicals Co.), and H_3PO_4 (85%, Nakarai tesque Co.) were mixed well. A 35 g batch was melted in a platinum crucible at 1100 °C for 15 min in an electric furnace. By pouring melts onto a steel plate,

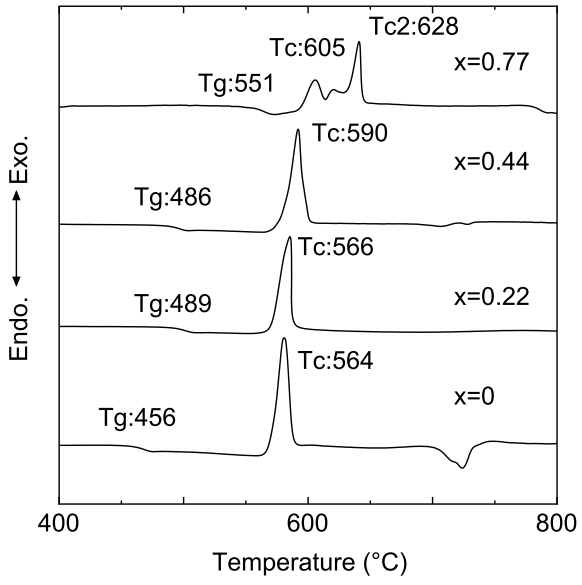

Fig. 2. DTA patterns of $Na_{2-x}Fe_{1+0.5x}P_2O_7$ precursor glasses with $x = 0$, 0.22, 0.44, and 0.77 in air. The heating rate was 10 K/min.

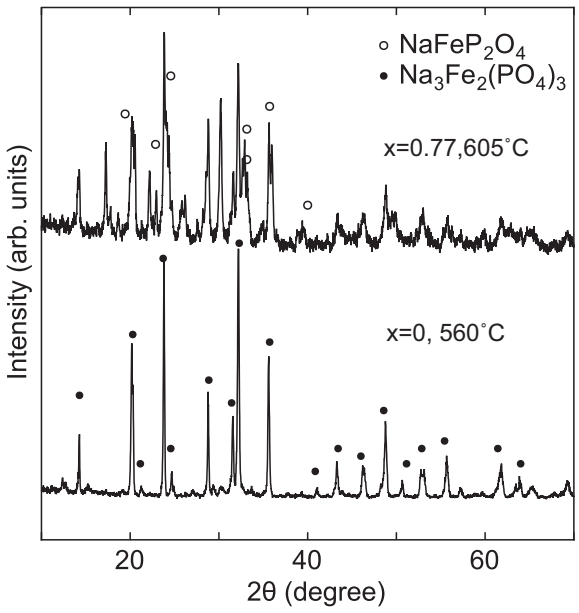

Fig. 3. Powder XRD patterns for $Na_{2-x}Fe_{1+0.5x}P_2O_7$ glass-ceramics ($x = 0$ and 0.77) obtained by heat treatments for 3 h in air.

black-colored precursor glasses were successfully formed. The glass transition and crystallization temperatures were determined by differential thermal analysis (DTA, Rigaku TG-8120). The glass compositions were determined by ICP spectroscopy (ICP-AES, SII SPS4000). [14] Glass powder of 2 μm diameter was obtained by using a planetary ball mill (Fritsch premium line P-7). Glass-ceramics were prepared by heat treatments in a tubular electric furnace with 5%H_2–95% Ar gas flows. The gas flow rate was 100 ml/min. To reduce Fe^{3+} to Fe^{2+} ions in the precursor glasses, 10 wt.% citric acid was added to glass powders. The amount of residual carbon content was determined by thermogravimetric analysis (TG-DTA, Rigaku TG-8120). Powder X-ray diffraction (XRD, Rigaku Ultima IV) employing Cu-Kα radiation was used to identify the crystalline phase in glass-ceramic powders. Morphologies of

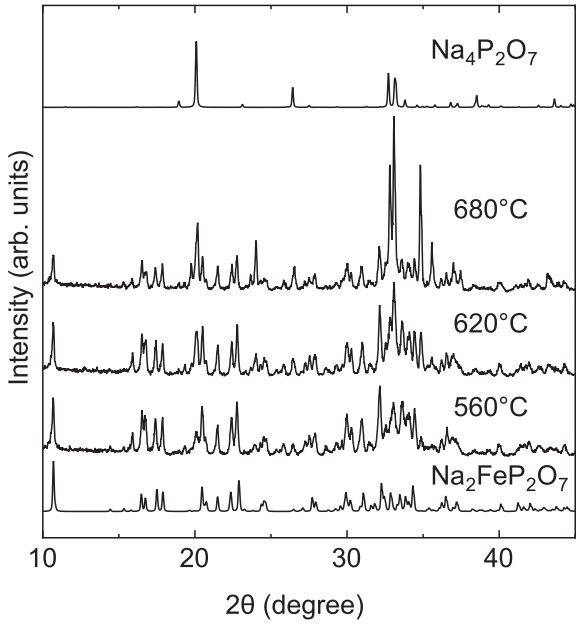

Fig. 4. Powder XRD patterns for $Na_2FeP_2O_7$ glass-ceramics heat-treated at various temperatures for 3 h in 5%H_2–95% Ar gas flows. The citric acid was added to the precursor glass powders prior to the crystallization.

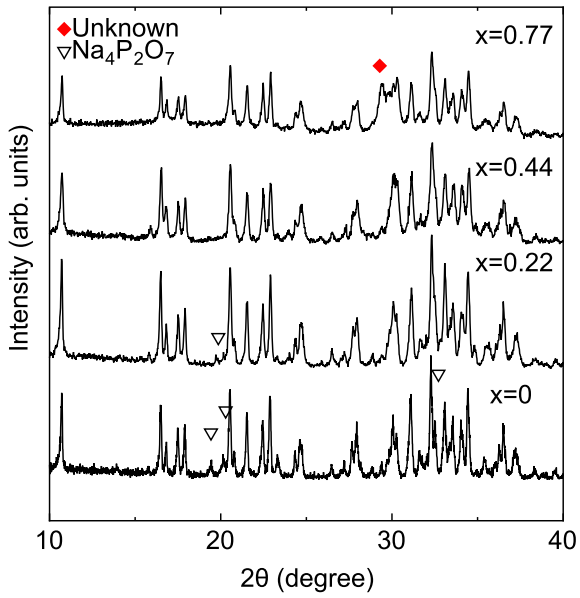

Fig. 5. Powder XRD patterns for $Na_{2-x}Fe_{1+0.5x}P_2O_7$ glass-ceramics ($x = 0$, 0.22, 0.44, and 0.77) heat-treated at crystallization peak temperatures for 3 h in 5%H_2–95% Ar gas flows. The citric acid was added to the precursor glass powders prior to the crystallization.

glass-ceramics/carbon composites were observed by a scanning electron microscope (SEM, Keyence VE-8800). Elemental microanalysis in a micro-scale level in glass-ceramics was performed with wavelength dispersive X-ray analysis (Shimazu Co., EPMA-1600). Cathode electrodes were fabricated from a mixture of active material, polyvinylidene fluoride (PVDF) and conductive carbon black in a weight ratio of 85:5:10. N-Methylpyrrolidone (NMP) was used to make slurry of their mixtures. After homogenization, slurry was coated on a thin aluminum foil and dried at 100 °C for 10 h in a vacuum oven. Electrodes were then pressed and disks were punched out as 16 mm ϕ. Electrochemical cells were prepared using coin-type cells. Sodium metal foils were used as anode, and glass filter papers (Advantec Co., GA-100) were used as separator. Test cells were assembled in an argon-filled glove box. The dew point of Ar atmosphere in the glove box was kept as −86 °C. The oxygen content was less than 0.33 ppm. The solution of 1 M-$NaPF_6$ (Tokyo Kasei Co.) in a mixture of ethylene carbonate (EC) and diethyl carbonate (DEC) (1:1, v/v, Kishida Chemicals Co.) was used as electrolyte. Cells were examined by using a battery testing system (Hokuto-denko Co.) at the charge/discharge current density of 1/10C (0.08 mA cm^{-2}) for the theoretical capacity of 97 mAh g^{-1} between 2.0 and 3.8 V.

3. Results

A glass-forming region for the sodium iron phosphate system taken from the international glass database (INTERGLAD Ver. 7, produced by New Glass Forum, Japan) [29] is shown in Fig. 1, in which the glass compositions examined in this study are marked as red open circle and typical cathode candidates [11,30,31] are also included. By means of ICP spectroscopy [14] the chemical composition of precursor is almost identical with batch compositions. The compositions of $Na_{2-x}Fe_{1+0.5x}P_2O_7$ glasses are very close to the borders of the glass formation region. We could not obtain uniform glass samples for the compositions corresponding to typical cathodes $Na_3Fe_2(PO_4)_3$ [30], $Na_4Fe_3(PO_4)_2P_2O_7$ [11] and $NaFePO_4$ [31] by melt quenching. On the other hand, we obtained uniform black colored glass samples for the compositions of $Na_{2-x}Fe_{1+0.5x}P_2O_7$ ($x = 0$–0.77) by pouring melts onto a steel plate.

Fig. 2 shows the DTA patterns of $Na_{2-x}Fe_{1+0.5x}P_2O_7$ precursor glasses. We determined glass transition onset T_g and top of crystallization peak T_c respectively. As shown in Fig. 2, all glass samples exhibit endothermic dips due to the glass transition and exothermic peaks corresponding to crystallization. With increasing x parameter in $Na_{2-x}Fe_{1+0.5x}P_2O_7$, the glass transition temperature increased

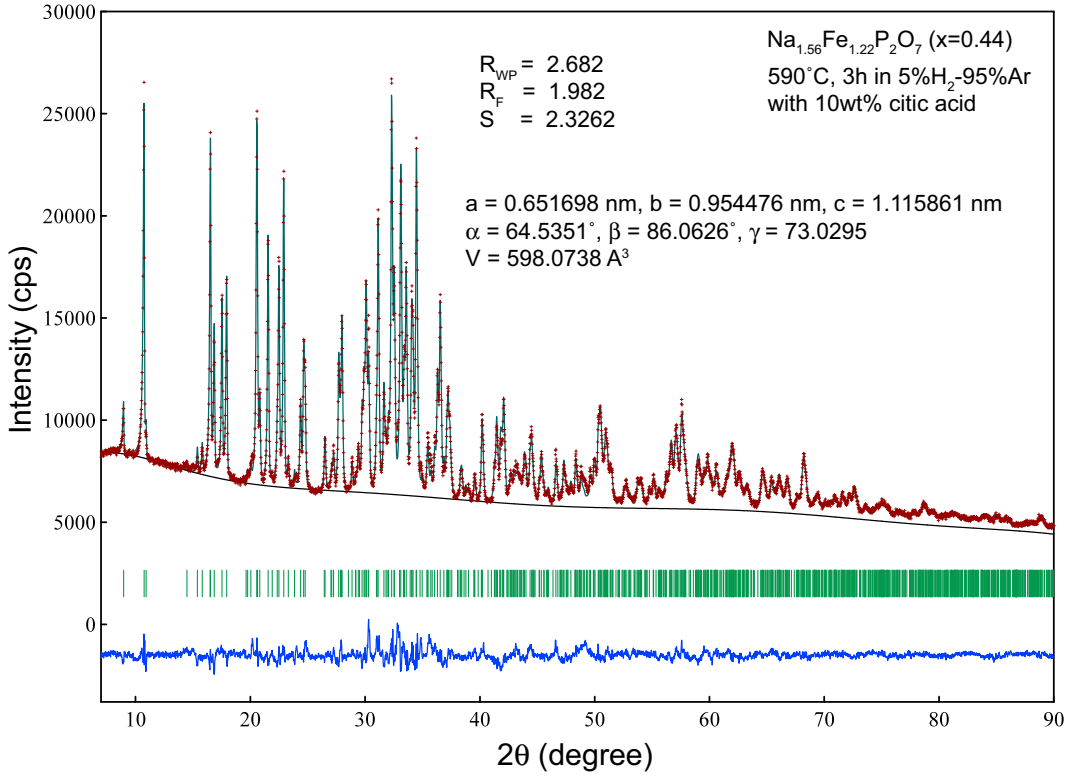

Fig. 6. X-ray Rietveld analysis for $Na_{1.56}Fe_{1.22}P_2O_7$ glass-ceramics. The initial structure model was applied by using the data reported in Ref. [28].

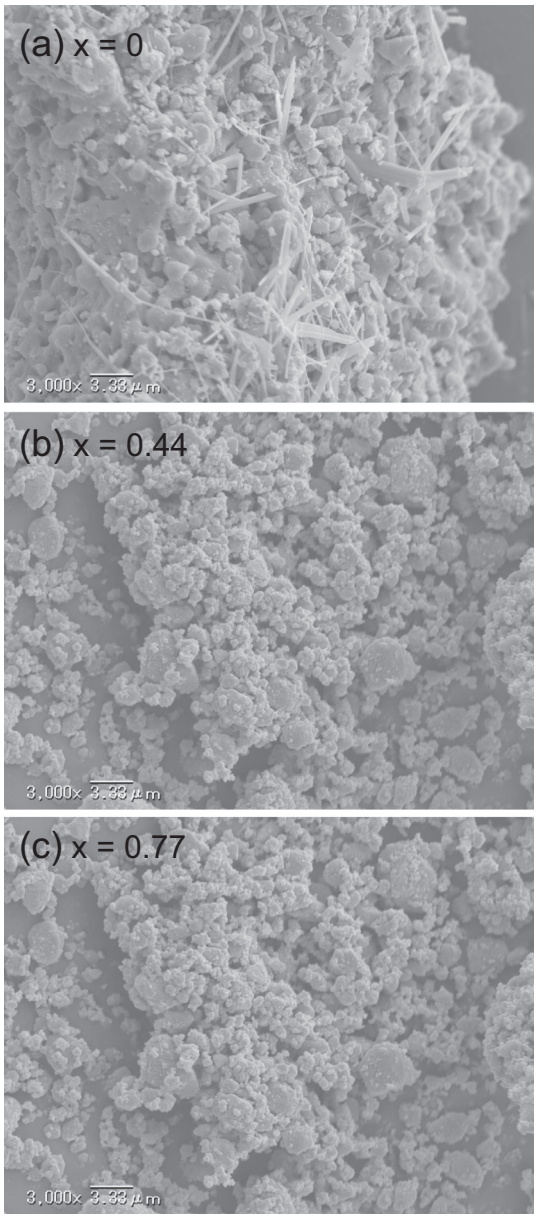

Fig. 7. SEM images for $Na_{2-x}Fe_{1+0.5x}P_2O_7$ glass-ceramic powders with (a) $x = 0$, (b) $x = 0.44$, and (c) $x = 0.77$.

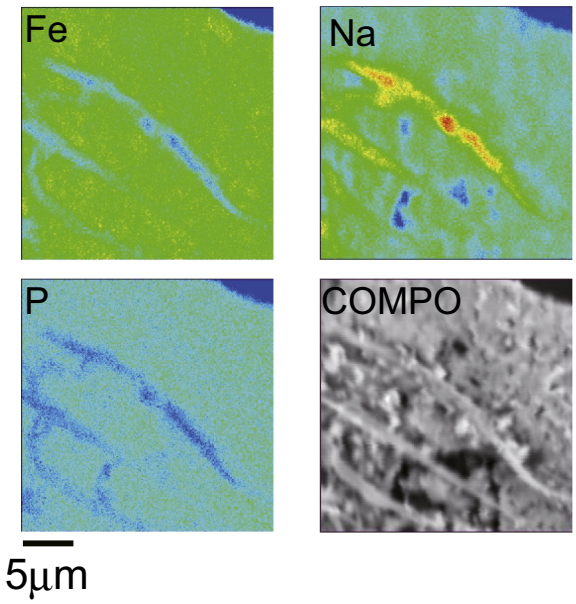

Fig. 8. EPMA element maps for $Na_2FeP_2O_7$ glass-ceramics with needle-shaped crystals.

gradually. In the previous studies [12,14,21], the valence state of iron in $Na_2FeP_2O_7$ and $LiFePO_4$ precursor glasses was found to be Fe^{3+} mainly. First we checked the crystalline phase in the glass-ceramics ($x = 0$ and 0.77) obtained by heat treatments in air. The heat treatment temperature was 560 °C for the glass with $x = 0$ and 605 °C for the glass with $x = 0.77$, which correspond to the crystallization peak temperatures determined by DTA analysis. The heat treatment time was kept for 3 h in each sample. Fig. 3 shows the powder XRD patterns for the glass-ceramics obtained. The formation of NASICON like $Na_3Fe(III)_2(PO_4)_3$ (ICDD #00-045-0319) and $NaFe(III)P_2O_7$ (ICDD #01-076-2174) crystalline phases is clearly observed.

10 wt.% citric acid as carbon source (i.e., reducing agent for Fe^{3+}) was added to the precursor glass powders, and the mixtures were heat-treated at some temperatures of 560, 620, and 680 °C for 3 h in air. Fig. 4 shows the powder XRD patterns for the heat-treated samples with $x = 0$, indicating that the main crystalline phase is triclinic $P\bar{1}$ phase. The formation of $Na_4P_2O_7$ phase is also detected as byproduct, and the intensity of its diffraction peaks increases with increasing heat treatment temperature.

The glass-ceramics with different chemical compositions of $Na_{2-x}Fe_{1+0.5x}P_2O_7$ with $x = 0$, 0.22, 0.44, and 0.77 were fabricated, in which the precursor glasses were heat-treated at crystallization peak temperature determined by DTA curve (Fig. 2) for 3 h in a tubular furnace with 5%H_2–95% Ar gas flow. Fig. 5 shows the powder XRD patterns for the heat-treated samples. The formation of $Na_4P_2O_7$ is detected in the samples with $x = 0$ and $x = 0.22$. In the sample with $x = 0.44$, any byproducts did not appear and the formation of only $P\bar{1}$ phase is confirmed. In the samples with $x = 0.77$, an unidentified crystalline phase is appeared besides the $P\bar{1}$ phase. From these results, we focus our attention on $Na_{2-x}Fe_{1+0.5x}P_2O_7$ glass with $x = 0.44$ more in detail. The composition of $x = 0.44$ accords with the crystal composition $Na_{3.12}Fe_{2.44}(P_2O_7)_2$ ($Na_{1.56}Fe_{1.22}P_2O_7$) proposed by Angenault et al. [28]. We determined the crystal structure parameters of the $P\bar{1}$ phase formed in the glass-ceramics with $x = 0.44$ using the Rietveld analysis (RIETAN-FP software) [32]. The results for the refined XRD pattern are shown in Fig. 6. In this analysis, the initial structure model was applied by using the data reported by Angenault et al. [28]. The lattice parameters for triclinic $P\bar{1}$ phase crystals in the glass-ceramics were calculated to be $a = 0.65169$ nm, $b = 0.95447$ nm, $c = 1.11586$ nm, $\alpha = 64.53°$, $\beta = 86.06°$, $\gamma = 73.02°$, and $V = 598$ Å^3. These values are close to those ($a = 0.6424$ nm, $b = 0.9440$ nm, $c = 1.0981$ nm, $\alpha = 64.77°$, $\beta = 86.21°$, $\gamma = 73.13°$, and $V = 575$ Å^3) reported by Angenault et al. [28]. Fig. 7 shows the SEM images for glass-ceramic powders with (a) $x = 0$, (b) $x = 0.44$, and (c) $x = 0.77$. Grains with a particle size of several micrometers are observed. In particular, it is noted that needle-shaped crystals are present at the surface of the sample with $x = 0$ (Fig. 7(a)). We found that these needle-shaped crystals dissolve easily in water. Fig. 8 shows the EPMA element maps for the needle-shaped crystals.

Fig. 9 shows the charge and discharge profiles from the first to fifth times for cathodes fabricated by using $Na_{2-x}Fe_{1+0.5x}P_2O_7$ glass-ceramics. The current density was fixed as 0.08 mA/cm^2 which corresponds to the 1/10C rate in $Na_2FeP_2O_7$. An oxidation–reduction equilibrium plateau between Fe^{2+} and Fe^{3+} in the $P\bar{1}$ phase crystals was confirmed in all compositions. The reversible discharge capacity in the sample with $x = 0.44$ was 83 mAh/g, whereas the sample with $x = 0.77$ showed the discharge capacity of 50 mAh/g.

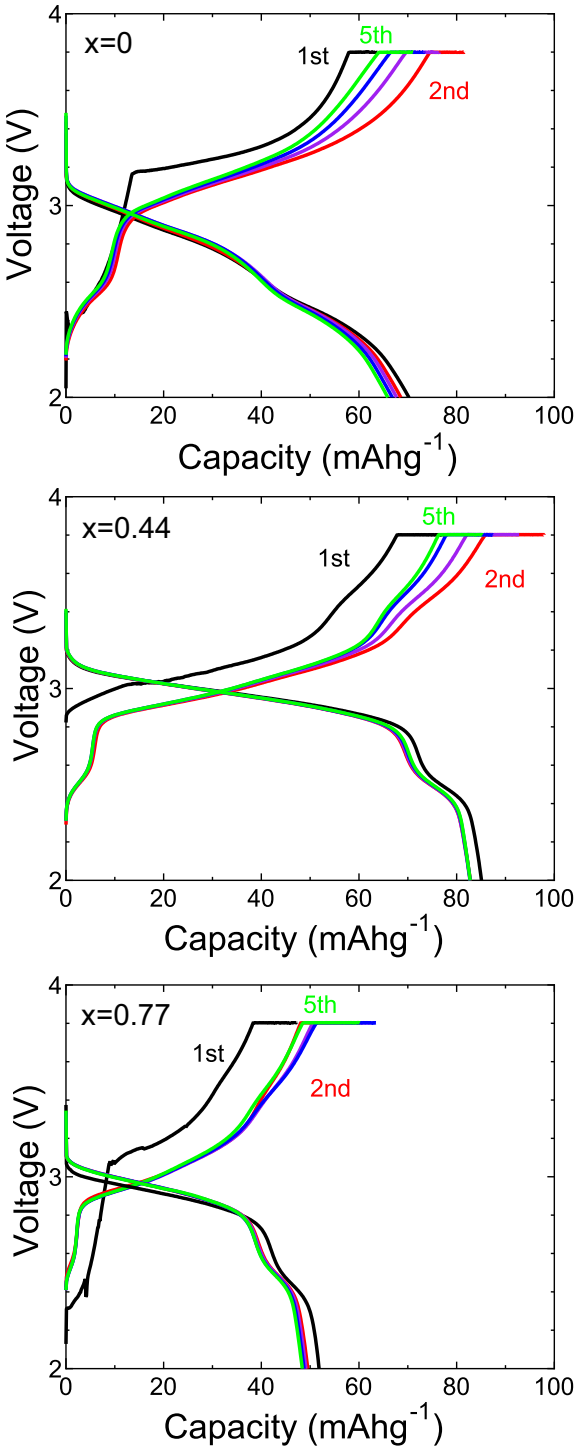

Fig. 9. Charge and discharge profiles from the first to five times for cathodes fabricated by using $Na_{2-x}Fe_{1+0.5x}P_2O_7$ glass-ceramics with $x = 0$, 0.44, and 0.77. Testing coin cells consist of glass-ceramic cathode and sodium metal anode.

4. Discussion

As shown in Fig. 2 and Fig. 3, we confirmed crystallization behavior in air and H_2-Ar mixture gas respectively. These results demonstrate that the valence of Fe^{3+} ions in the precursor glasses must be reduced to Fe^{2+} ions during heat treatments (i.e., crystallization) in order to form $Na_{2-x}Fe(II)_{1+x/2}P_2O_7$ being the target crystals in this study.

We confirmed thermal decomposition of $Na_2FeP_2O_7$ glass at high temperature as shown in Fig. 4. It should be pointed out that other research groups also report the formation (several percent) of byproducts in the solid-state reaction process [15,16]. Anyway, the results shown in Fig. 4 suggest that it is important to control more strictly heat treatment condition or design more precisely chemical composition to fabricate glass-ceramics with only (pure) $P\bar{1}$ phase. Because sodium element is highly concentrated in the needle-shaped crystals as shown in Fig. 7 and Fig. 8, it would be reasonable to conclude that needle-shaped crystals are $Na_4P_2O_7$, which is confirmed in XRD patterns (Fig. 5).

We expected that electro-chemical discharge capacity will increase with increasing of x parameter in Eq. (1). According to Eq. (1), the theoretical discharge capacity in $Na_{2-x}Fe_{1+0.5x}P_2O_7$ crystals increases with increasing x, e.g., 118 mAh/g in $Na_{3.12}Fe_{2.44}(P_2O_7)_2$ with $x = 0.44$. Furthermore, it is obvious that the discharge capacity depends on the volume fraction of the $P\bar{1}$ phase crystals. At this moment, the volume fraction of $Na_{2-x}Fe_{1+0.5x}P_2O_7$ crystals in the glass-ceramics with $x = 0.44$ has not been determined. Further studies, which lead to the increase in the volume fraction of $Na_{2-x}Fe_{1+0.5x}P_2O_7$ crystals and in the discharge capacity, will be required.

5. Conclusion

We examined the glass formation and crystallization behavior in Na_2O-Fe_2O_3-P_2O_5 system in order to develop glass-ceramic cathodes as sodium ion batteries. The glasses with the compositions of $Na_{2-x}Fe_{1+0.5x}P_2O_7$ with $x = 0$, 0.44, and 0.77 were obtained, and glass-ceramics consisting of $Na_{1.56}Fe_{1.22}P_2O_7$ ($x = 0.44$) crystals with a triclinic $P\bar{1}$ phase were fabricated by controlling heat treatment temperature, time, and atmosphere. The glass-ceramics with $x = 0.44$ showed a reversible discharge capacity of 83 mAh/g. We propose that the glass-ceramic processing is one of the suitable ways to produce sodium ion battery cathodes without using precious Fe^{2+} derived raw materials.

Acknowledgment

This study was supported by the Grant-in-Aid for Scientific Research from the Ministry of Education, Science, Sport, Culture, and Technology, Japan (Grant Nos. 23246114, 24656379, and 25288105), Research Corroboration Project to develop high performance secondary battery materials between Nagaoka University Technology and Nippon Electric Glass Co. Ltd. and Program for High Reliable Materials Design and Manufacturing in Nagaoka University of Technology. One of the authors (T. Honma) was financially supported by Izumi Science and Technology Foundation (H24-J-127).

References

[1] C. Fouassier, G. Matejka, J.-M. Reau, P. Hagenmuller, Sur de nouveaux bronzes oxygénés de formule Na_xCoO_2 le système cobalt–oxygène–sodium, J. Solid State Chem. 6 (4) (1973) 532–537, http://dx.doi.org/10.1016/S0022-4596(73)80011-8.
[2] J.-J. Braconnier, C. Delmas, C. Fouassier, P. Hagenmuller, Comportement electrochimique des phases Na_xCoO_2, Mater. Res. Bull. 15 (12) (1980) 1797–1804, http://dx.doi.org/10.1016/0025-5408(80)90199-3.
[3] S. Okada, Y. Takahashi, T. Kiyabu, T. Doi, J.-I. Yamaki, T. Nishida, Layered Transition Metal Oxides as Cathodes for Sodium Secondary Battery, Meeting Abstracts, no. 4, The Electrochemical Society, 2006, p. 201, (http://ma.ecsdl.org/content/MA2006-02/4/201.short).
[4] Z. Lu, J. Dahn, In situ X-ray diffraction study of P_2 $Na_{2/3}[Ni_{1/3}Mn_{2/3}]O_2$, J. Electrochem. Soc. 148 (11) (2001) A1225–A1229, http://dx.doi.org/10.1149/1.1407247.
[5] D. Kim, E. Lee, M. Slater, W. Lu, S. Rood, C.S. Johnson, Layered $Na[Ni_{1/3}Fe_{1/3}Mn_{1/3}]O_2$ cathodes for Na-ion battery application, Electrochem. Commun. 18 (2012) 66–69, http://dx.doi.org/10.1016/j.elecom.2012.02.020.
[6] N. Yabuuchi, M. Kajiyama, J. Iwatate, H. Nishikawa, S. Hitomi, R. Okuyama, R. Usui, Y. Yamada, S. Komaba, P_2-type $Na_x[Fe_{1/2}Mn_{1/2}]O_2$ made from earth-abundant elements for rechargeable Na batteries, Nat. Mater. 11 (6) (2012) 512–517, http://dx.doi.org/10.1038/nmat3309.
[7] P. Vassilaras, X. Ma, X. Li, G. Ceder, Electrochemical properties of monoclinic $NaNiO_2$, J. Electrochem. Soc. 160 (2) (2013) A207–A211, http://dx.doi.org/10.1149/2.023302jes.
[8] J. Gopalakrishnan, K.K. Rangan, Vanadium phosphate ($V_2(PO_4)_3$): a novel NASICON-type vanadium phosphate synthesized by oxidative deintercalation of sodium from

sodium vanadium phosphate ($Na_3V_2(PO_4)_3$), Chem. Mater. 4 (4) (1992) 745–747, http://dx.doi.org/10.1002/chin.199244030.

[9] Y. Kawabe, N. Yabuuchi, M. Kajiyama, N. Fukuhara, T. Inamatsu, R. Okuyama, I. Nakai, S. Komaba, A comparison of crystal structures and electrode performance between Na_2FePO_4F and $Na_2Fe_{0.5}Mn_{0.5}PO_4F$ synthesized by solid-state method for rechargeable Na-ion batteries, Electrochemistry 80 (2) (2012) 80–84, http://dx.doi.org/10.5796/electrochemistry.80.80 (URL http://joi.jlc.jst.go.jp/JST.JSTAGE/electrochemistry/80.80?from=CrossRef).

[10] R. Gover, a. Bryan, P. Burns, J. Barker, The electrochemical insertion properties of sodium vanadium fluorophosphate, $Na_3V_2(PO_4)_2F_3$, Solid State Ionics 177 (17-18) (2006) 1495–1500, http://dx.doi.org/10.1016/j.ssi.2006.07.028 (URL http://linkinghub.elsevier.com/retrieve/pii/S0167273806004024).

[11] H. Kim, I. Park, D.-H. Seo, S. Lee, S.-W. Kim, W.J. Kwon, Y.-U. Park, C.S. Kim, S. Jeon, K. Kang, New iron-based mixed-polyanion cathodes for lithium and sodium rechargeable batteries: combined first principles calculations and experimental study, J. Am. Chem. Soc. 134 (25) (2012) 10369–10372, http://dx.doi.org/10.1021/ja3038646 (URL http://www.ncbi.nlm.nih.gov/pubmed/22667817).

[12] T. Honma, T. Togashi, N. Ito, T. Komatsu, Fabrication of $Na_2FeP_2O_7$ glass-ceramics for sodium ion battery, J. Ceram. Soc. Jpn. 120 (1404) (2012) 344–346, http://dx.doi.org/10.2109/jcersj2.120.344 (URL http://japanlinkcenter.org/DN/JST.JSTAGE/jcersj2/120.344?lang=en&from=CrossRef&type=abstract).

[13] T. Honma, T. Komatsu, J. Ikejiri, H. Yamauchi, Cathode Active Material for Sodium Secondary Battery and Method for Manufacturing the Cathode Active Material for Sodium Secondary Battery, wO Patent App. PCT/JP2013/056,272, 2013. (Sep. 12, URL https://www.google.com/patents/WO2013133369A1?cl=en).

[14] T. Honma, N. Ito, T. Togashi, A. Sato, T. Komatsu, Triclin ic $Na_{2-x}Fe_{1+x/2}P_2O_7$/C glass-ceramics with high current density performance for sodium ion battery, J. Power Sources 227 (2013) 31–34, http://dx.doi.org/10.1016/j.jpowsour.2012.11.030 (URL http://linkinghub.elsevier.com/retrieve/pii/S0378775312017041).

[15] H. Kim, R.a. Shakoor, C. Park, S.Y. Lim, J.-S. Kim, Y.N. Jo, W. Cho, K. Miyasaka, R. Kahraman, Y. Jung, J.W. Choi, $Na_2FeP_2O_7$ as a promising iron-based pyrophosphate cathode for sodium rechargeable batteries: a combined experimental and theoretical study, Adv. Funct. Mater. 23 (9) (2012) 1147–1155, http://dx.doi.org/10.1002/adfm.201201589 (URL http://doi.wiley.com/10.1002/adfm.201201589).

[16] P. Barpanda, T. Ye, S.-i. Nishimura, S.-C. Chung, Y. Yamada, M. Okubo, H. Zhou, A. Yamada, Sodium iron pyrophosphate: a novel 3.0v iron-based cathode for sodium-ion batteries, Electrochem. Commun. 24 (2012) 116–119, http://dx.doi.org/10.1016/j.elecom.2012.08.028 (URL http://linkinghub.elsevier.com/retrieve/pii/S1388248112003591).

[17] C.-Y. Chen, K. Matsumoto, T. Nohira, C. Ding, T. Yamamoto, R. Hagiwara, Charge–discharge behavior of a Na2FeP2O7 positive electrode in an ionic liquid electrolyte between 253 and 363 K, Electrochim. Acta 133 (1 July 2014) 583–588, http://dx.doi.org/10.1016/j.electacta.2014.04.038.

[18] C.-Y. Chen, K. Matsumoto, T. Nohira, R. Hagiwara, Y. Orikasa, Y. Uchimoto, Pyrophosphate $Na_2FeP_2O_7$ as a low-cost and high-performance positive electrode material for sodium secondary batteries utilizing an inorganic ionic liquid, J. Power Sources 246 (2014) 783–787, http://dx.doi.org/10.1016/j.jpowsour.2013.08.027 (URL http://linkinghub.elsevier.com/retrieve/pii/S0378775313013670).

[19] Y.H. Jung, C.H. Lim, J.-H. Kim, D.K. Kim, Na2FeP2O7 as a positive electrode material for rechargeable aqueous sodium-ion batteries, RSC Advances 4 (2014) 9799–9802, http://dx.doi.org/10.1039/C3RA47560C.

[20] T. Honma, K. Hirose, T. Komatsu, T. Sato, S. Marukane, Fabrication of $LiFePO_4$/carbon composites by glass powder crystallization processing and their battery performance, J. Non-Cryst. Solids 356 (52-54) (2010) 3032–3036, http://dx.doi.org/10.1016/j.jnoncrysol.2010.05.079 (URL http://linkinghub.elsevier.com/retrieve/pii/S002230931000459X).

[21] K. Nagamine, K. Oh-Ishi, T. Honma, T. Komatsu, Formation mechanism of $LiFePO_4$ in crystallization of lithium iron phosphate glass particles, J. Ceram. Soc. Jpn. 120 (1401) (2012) 193–198, http://dx.doi.org/10.2109/jcersj2.120.193 (URL http://japanlinkcenter.org/JST.JSTAGE/jcersj2/120.193?from=CrossRef&type=abstract).

[22] T. Nagakane, H. Yamauchi, K. Yuki, M. Ohji, a. Sakamoto, T. Komatsu, T. Honma, M. Zou, G. Park, T. Sakai, Glass-ceramic $LiFePO_4$ for lithium-ion rechargeable battery, Solid State Ionics 206 (2012) 78–83, http://dx.doi.org/10.1016/j.ssi.2011.10.017 (URL http://linkinghub.elsevier.com/retrieve/pii/S0167273811005248).

[23] T. Honma, K. Nagamine, T. Komatsu, Fabrication of olivine-type $LiMn_xFe_{1-x}PO_4$ crystals via the glass-ceramic route and their lithium ion battery performance, Ceram. Int. 36 (3) (2010) 1137–1141, http://dx.doi.org/10.1016/j.ceramint.2009.10.003 (URL http://linkinghub.elsevier.com/retrieve/pii/S0272884209003861).

[24] K. Nagamine, T. Honma, T. Komatsu, A fast synthesis of $Li_3V_2(PO_4)_3$ crystals via glass-ceramic processing and their battery performance, J. Power Sources 196 (22) (2011) 9618–9624, http://dx.doi.org/10.1016/j.jpowsour.2011.06.094 (URL http://linkinghub.elsevier.com/retrieve/pii/S0378775311013310).

[25] K. Nagamine, T. Honma, T. Komatsu, Fabrication of $LiVOPO_4$/carbon composite via glass-ceramic processing, IOP Conf. Ser. Mater. Sci. Eng. 21 (2011) 012021, http://dx.doi.org/10.1088/1757-899X/21/1/012021 (URL http://stacks.iop.org/1757-899X/21/i=1/a=012021?key=crossref.2d1dfa25d88a1b1f0830335a6baa1d1c).

[26] H. Yamauchi, G. Park, T. Nagakane, T. Honma, T. Komatsu, T. Sakai, a. Sakamoto, Performance of lithium-ion battery with tin-phosphate glass anode and its characteristics, J. Electrochem. Soc. 160 (10) (2013) A1725–A1730, http://dx.doi.org/10.1149/2.049310jes (URL http://jes.ecsdl.org/cgi/doi/10.1149/2.049310jes).

[27] T. Honma, T. Togashi, H. Kondo, T. Komatsu, H. Yamauchi, A. Sakamoto, T. Sakai, Tin-phosphate glass anode for sodium ion batteries, APL Mater. 1 (5) (2013) 052101, http://dx.doi.org/10.1063/1.4826938 (URL http://link.aip.org/link/AMPADS/v1/i5/p052101/s1&Agg=doi).

[28] J. Angenault, J.C. Couturier, M. Quarton, Structure of $Na_{3.12}Fe_{2.44}(P_2O_7)_2$, Eur. J. Solid State Inorg. Chem. 32 (1995) 335–343.

[29] Glass data-base: INTERGLAD, URL http://www.newglass.jp/intergladn/gaiyo/infoe.html .

[30] I. Lyubutin, O. Melnikov, S. Sigaryov, V. Terziev, Phase transitions in $Na_3Fe_2(PO_4)_3$: an inside view, Solid State Ionics 31 (3) (1988) 197–201, http://dx.doi.org/10.1016/0167-2738(88)90268-8.

[31] P. Moreau, D. Guyomard, J. Gaubicher, F. Boucher, Structure and stability of sodium intercalated phases in olivine $FePO_4$, Chem. Mater. 22 (14) (2010) 4126–4128, http://dx.doi.org/10.1021/cm101377h (URL http://pubs.acs.org/doi/abs/10.1021/cm101377h).

[32] F. Izumi, K. Momma, Three-dimensional visualization in powder diffraction, Solid State Phenom. 130 (2007) 15–20, http://dx.doi.org/10.4028/www.scientific.net/SSP.130.15.